



Contents lists available at ScienceDirect

## Spectrochimica Acta Part A: Molecular and Biomolecular Spectroscopy

journal homepage: [www.elsevier.com/locate/saa](http://www.elsevier.com/locate/saa)

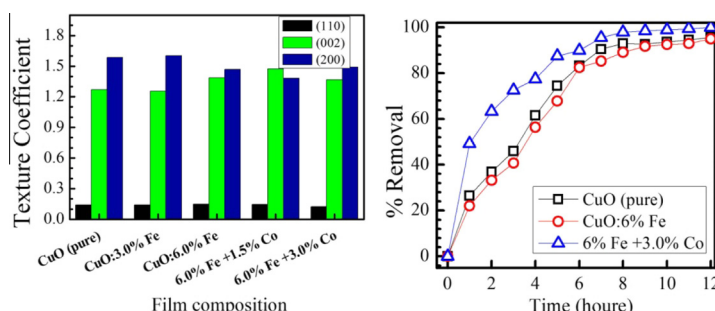
## Structural, optical and photocatalytic properties of Fe and (Co, Fe) co-doped copper oxide spin coated films

A.M. El Sayed<sup>a,\*</sup>, Mohamed Shaban<sup>b</sup><sup>a</sup> Department of Physics, Faculty of Science, Fayoum University, Fayoum 63514, Egypt<sup>b</sup> Nanophotonics and Applications (NPA) Lab, Department of Physics, Faculty of Science, Beni-Suef University, Beni-Suef 62514, Egypt

## HIGHLIGHTS

- CuO films doped with Fe and co-doped with Co have been prepared by spin coating.
- The structural properties and film thickness have been evaluated by XRD and FE-SEM.
- The influence of doping ratio on the optical constants of the films were reported.
- The photocatalytic activity and MB dye removal of the CuO films were studied.

## GRAPHICAL ABSTRACT



## ARTICLE INFO

## Article history:

Received 21 November 2014

Received in revised form 22 April 2015

Accepted 4 May 2015

Available online 7 May 2015

## Keywords:

CuO  
 Nanostructured films  
 Co-doping  
 Band gap tuning  
 Optical constants  
 Dye removal

## ABSTRACT

Copper oxide films with composition  $\text{Cu}_{1-x-y}\text{Fe}_x\text{Co}_y\text{O}$  (where  $x \leq 0.06$  and  $y \leq 0.03$  in a molar ratio) and thickness of about 2  $\mu\text{m}$  were spin coated onto ultrasonically cleaned glass substrates. These films were annealed at 500 °C in the air. XRD results show that films are CuO of polycrystalline and monoclinic structures without the detection of any Fe or Co traces. The average crystallite size of pure CuO is 20.44 nm reduced to 18.72 nm after Fe doping, then increased to 26.82 nm due to the co-doping with Co atoms. The optical band gap blue-shifted from 2.15 eV to 2.3 eV followed by red-shift to 2.15 eV after the Co incorporation. The influence of Fe doping and Co co-doping on the optical constants of CuO films as well as the photocatalytic removal of methylene blue (MB) dye is reported. The correlations between the structural modifications and the resultant optical properties are discussed. The obtained results of the fabricated system are compared with those of similar materials.

© 2015 Elsevier B.V. All rights reserved.

## Introduction

Among the transition metal oxides, the nanostructured copper oxides have attracted much interest due to the promising applications of these materials in the applied science and technology. Cuprous oxide,  $\text{Cu}_2\text{O}$ , is a *p*-type semiconductor with a direct band gap around 2.2 eV [1,2] and exhibits high hole mobility theoretically exceeding 100  $\text{cm}^2/(\text{V s})$  [3]. Thus,  $\text{Cu}_2\text{O}$  is a very promising

candidate for solar cell applications, i.e. a suitable material for photovoltaic energy conversion [4,5]. Cupric oxide, CuO, has a band gap of 1.2–2.1 eV and exhibits *p*-type conductivity due to the excess of oxygen or copper vacancies in its structure [1,5–12]. However, the existence of oxygen vacancies and/or Cu phase may lead to *n*-type behavior for CuO [7,13,14]. The transition metal copper (Cu; [Ar]  $3d^{10}4s^1$ ) is one of the most abundant elements in the Earth's crust. In addition, CuO shows good electronic and thermal properties, chemical stability and electrochemical activity with a longer shelf life compared to organic antimicrobial agents [15]. Beside the low production cost and non-toxicity, CuO has a high dielectric constant and a refractive index of 1.4. Therefore, CuO

\* Corresponding author. Tel.: +966 502608368.

E-mail addresses: [ams06@fayoum.edu.eg](mailto:ams06@fayoum.edu.eg), [adel\\_sayed\\_2020@yahoo.com](mailto:adel_sayed_2020@yahoo.com) (A.M. El Sayed).

thin films have been widely used for various applications such as humidity and gas sensors [16–22], supercapacitors [23], solar energy applications [24–26], photocatalytic, antimicrobial and anticancer activities [5,27–31], lithium ion batteries [2,32], spintronics and high TC superconductors [33–38], nanofluids and heat transfer applications [39,40].

The chemical and physical properties of most of the nanoscale materials are strictly depend on their sizes and morphologies. Therefore, considerable efforts have been made to synthesize various CuO nanostructures with well-defined morphologies via applying different synthesizing techniques. Preparation of CuO microspheres [19], nanoneedles [25], nanoparticles (NPs) [31,41–46], nanowires [18,47], cauliflower-like, nanobelt-shaped, feather-like, network-like structure [21,44], and flower-like [10,29,48] CuO have been reported. Sohrabnezhad et al. [15] prepared spherical CuO NPs of size 3–5 nm via a thermal decomposition method. Sankar et al. [28] synthesized rod-shaped CuO with an average size of 140 nm from *Carica papaya* leaves. Sivaraj et al. prepared CuO NPs from *Acalypha indica* [30] and *Tabernaemontana divaricate* leaves [31] via green chemistry approaches. Sabbaghan et al. [12] were able to control the morphology of CuO NPs by adjusting the amounts of NaOH and the ionic liquids additives. Chand et al. [49] converted the hydrothermally prepared CuO nanorods into rectangular nanoflakes only by adjusting the pH value of the solution. Simultaneously, the CuO thin films have been fabricated using various chemical and physical methods including thermal oxidation of Cu films [13], reactive DC sputtering [16], pulsed laser deposition (PLD) [20], colloidal solution [23] and solution combustion [29] methods, sol–gel spin coating [17,24], RF magnetron sputtering [34], sol–gel dip coating [9,11,50], spray pyrolysis [14,51], flame spray pyrolysis followed by spin coating [44], and successive ionic layer adsorption and reaction (SILAR) method [52]. Among these techniques, the sol–gel chemistry together with the spin coating method is preferred due to its simplicity, massive production, safety, environmentally friendly, controllability over the composition and film thickness. Also, this technique has been used to obtain high quality thin films of tens of cm<sup>2</sup> areas on both crystalline and amorphous surfaces [46,53].

Doping with metallic atoms can be used to improve the physical and chemical properties of CuO thin films in order to satisfy the particular needs and uses. The effects of In (up to 10%) on the optical band gap and the conduction mechanism of the dip coated CuO films have been reported [9,11]. CuO: 15% Ru films exhibited a higher specific capacitance with larger potential window compared to the un-doped CuO film [23]. The effects of Mn doping on the electrical and magnetic properties of CuO films have been reported by Zhang et al. [34,35]. Ehrman et al. [44] found that doping with 5% Li increases the conductivity of CuO films by two orders of magnitude due to the long lifetime of the photogenerated charge carriers. Gulen et al. [52] reported the increase in the band gap ( $E_g$ ) value of CuO films from 1.42 to 2.2 eV with increasing the Mn ratio up to 5%. The  $E_g$  values of the spray deposited CuO films increased from 1.66 to 1.96 eV when doped with 10% Fe and the magnetization at 300 K showed a hysteresis behavior with large coercivity [54]. Based on the above survey, there are few reports on the sol–gel spin coated CuO thin films. Also, to the best of our knowledge, this is the first report discusses the influence of Fe doping and Co co-doping on the structural, optical properties, optical constants, and photocatalytic activity of CuO films.

## Experimental details

### Films preparation

Pure, Fe-doped and Co-co-doped CuO films were prepared by sol–gel method and spin coating technique. The starting material

was Cu(II) acetate hydrate [Cu(COOCH<sub>3</sub>)<sub>2</sub>·H<sub>2</sub>O,  $M_w = 199.65$ , 98%, PRS Panreac, Spain] as a metal cation precursors. The solutions were prepared by dissolving 0.35 M of Cu(II) acetate hydrate in 2-methoxyethanol (CH<sub>3</sub>OCH<sub>2</sub>CH<sub>2</sub>OH, 99.8%, Aldrich). Then, 0.7 M of monoethanolamine (C<sub>2</sub>H<sub>7</sub>NO, 98%, Aldrich) was added to the solutions as a stabilizer. The Fe and Co sources were FeCl<sub>3</sub>·6H<sub>2</sub>O [ $M_w = 270.30$ , Nova Oleochem Limited] and Co(NO<sub>3</sub>)<sub>2</sub>·6H<sub>2</sub>O [ $M_w = 291.03$ , purity > 99%, Aldrich]. The additives were controlled to obtain the following compositions; CuO, Cu<sub>0.97</sub>Fe<sub>0.03</sub>O, Cu<sub>0.94</sub>Fe<sub>0.06</sub>O, Cu<sub>0.925</sub>Fe<sub>0.06</sub>Co<sub>0.015</sub>O, and Cu<sub>0.91</sub>Fe<sub>0.06</sub>Co<sub>0.03</sub>O. For simplicity, these compositions are named: CuO (pure), CuO: 3% Fe, CuO: 6% Fe, 6% Fe + 1.5% Co, 6% Fe + 3.0% Co, respectively. The solutions were stirred at 60 °C for 1 h and aged for more than 20 h at room temperature (RT). Before the spin coating process, the substrates were cleaned with dilute chromic acid and by sonication in acetone, ethanol, and deionized water for 10 min each. Then, the substrates were dried using air gun and baked at 100 °C for 20 min to remove any residual moisture. The precursor solutions spin-coated on the substrates at 3000 rpm for 30 s, followed by drying at 250 °C for 10 min on a hot plate. Spin coating and drying were repeated nine times to obtain the desired thickness. Finally, the films were annealed at 500 °C in air furnace.

### Measurements

For identification of phases and crystallographic properties of the as-prepared oxide films, X-ray diffraction (XRD, Philips X'PertPro MRD) using Cu  $K_\alpha$  radiation ( $\lambda = 1.5418 \text{ \AA}$ ) with a step 0.021, was used. Morphological and chemical composition studies of the fabricated nanostructure films were carried out using FE-SEM (model: ZEISS SUPRA 55 VP and ZEISS LEO, Gemini Column) equipped with an energy-dispersive X-ray spectroscopy (EDX). Optical spectra (reflectance and transmittance) in the spectral range from 300 to 1000 nm were measured using UV/VIS/NIR 3700 double beam Shimadzu spectrophotometer at RT. The films were dipped in an aqueous solution of 10 ppm methylene blue (MB) at RT to study the photocatalytic decomposition of MB. The experiment was carried out in the daytime between 11:00 am and 17:00 pm, during June, 2014, under the illumination of natural sunlight. The absorbance values were measured using UV-2100 Shimadzu spectrophotometer.

## Results and discussions

### Structural properties

Fig. 1 shows the XRD patterns of the copper oxide films synthesized by a spin coating method and annealed at 500 °C in air. All the diffraction peaks at  $2\theta = 32.463$ , 35.509, 38.567, 48.804, 53.2507, 58.1986, 61.579, 66.384, 67.987 and 75.109 are purely assigned to the (110), (002), (200), ( $\bar{2}02$ ), (020), (202), ( $\bar{1}13$ ), ( $\bar{3}11$ ), (220), and ( $22\bar{2}$ ) crystal planes, respectively. It can be seen that the films are polycrystalline and all the diffraction peaks belong to the CuO monoclinic (tenorite) phase that belong to the C2/c space group (JCPDS 48-1548). The intense and sharp diffraction peaks indicate that well crystallized CuO nanostructured films can be obtained under the synthetic conditions. There are no definite changes in the peaks position. There are no extra peaks corresponding to metallic Cu, Fe, and Co or the related phases of these metals (oxides or any ternary copper iron cobalt phases) in the doped CuO films. This suggested that Fe and Co atoms were effectively substituted Cu sites within CuO lattice without affecting the crystal structure of the parent material (CuO). Similar results were reported for Ni-doped CuO nanopowders [8], thin films of In-doped CuO prepared by sol–gel using the ethanol as a solvent [11], CuO

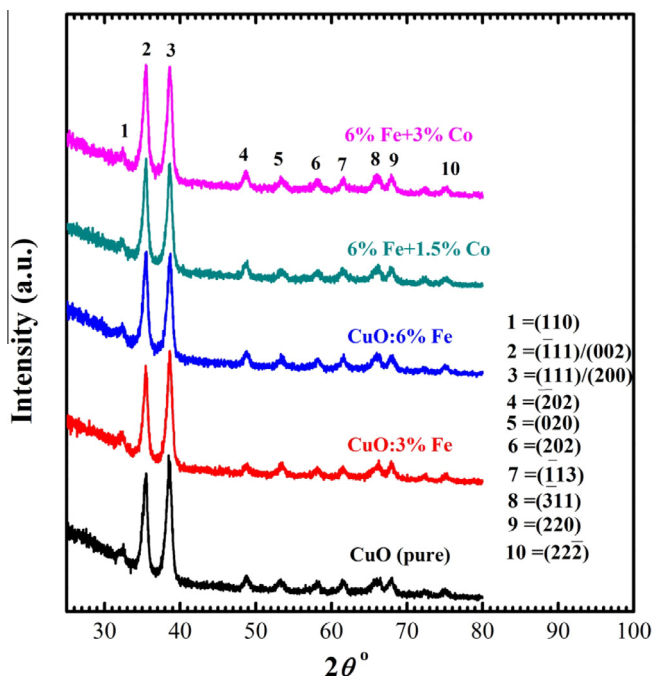


Fig. 1. XRD patterns of the sol-gel spin coated Fe- and Co-doped CuO films.

NPs prepared by a reflux method using pyridinium based ionic liquids [12], and for Mn-doped CuO nanoflakes [38]. However, another research group found weak signals correspond to  $\text{CuFe}_2\text{O}_4$  and NiO in the XRD of  $\text{Cu}_{0.9}\text{Fe}_{0.1}\text{O}$  and  $\text{Cu}_{0.8}\text{Ni}_{0.1}\text{Fe}_{0.1}\text{O}$  NPs, respectively [36].

The average crystallite sizes of the films were calculated from the peak widths, considering the first three peaks, using Scherer equation;  $C_s = 0.94\lambda/B\cos\theta$ . Where,  $C_s$  is the average crystallite size,  $\lambda$  is the used wavelength (1.546 Å for  $\text{Cu } K_{\alpha}$ ),  $B$  is the full-width at half-maximum (FWHM) intensity of the peaks after subtraction of the equipment broadening, and  $\theta$  is the diffraction angle. The  $B$  values for the planes (110), (002), and (200), as well as the  $C_s$  values, are listed in Table 1. The average crystallite size of the pure CuO is found to be 20.44 nm and decreases to 18.72 nm with increasing Fe doping ratio to 6.0%, indicating a small deterioration in the films' crystallinity. The decrease of  $C_s$  with increasing the doping ratio was also reported for the dip coated In-doped CuO films [9], the sol-gel prepared Zn-doped CuO NPs [46] and the spray pyrolyzed Zn-doped  $\text{TiO}_2$  films [55]. In addition, our results indicate that the co-doping of CuO films with Co increases the crystallite size to 26.82 nm. This means that the co-doping with Co enhances the grain growth of CuO. Similar results were reported for Mn-doped CuO nanoflakes prepared by a wet chemical method [38] and for the sol-gel prepared Cu-doped  $\text{TiO}_2$  NPs [56].

The lattice parameters  $a$ ,  $b$ ,  $c$  and the volume of the unit cell,  $V$ , of the CuO monoclinic structure were calculated using the following relations [11,51]:

$$\frac{1}{d^2} = \frac{1}{\sin^2 \beta} \left( \frac{h^2}{a^2} + \frac{k^2}{b^2} \sin^2 \beta + \frac{l^2}{c^2} - \frac{2hl \cos \beta}{ac} \right) \quad (1)$$

$$V = abc \sin \beta \quad (2)$$

The  $d$ -spacing ( $d$ ) values and the calculated  $a$ ,  $b$ ,  $c$ , and  $V$  values are listed in Table 1. These values are in a good agreement with the reported values in the literature [32,38]. It is observed from Table 1 that the variation of the doped CuO lattice parameters is not remarkable when compared with the un-doped CuO and do not follow a systematic trend with increasing the Fe and Co content. This indicates that the incorporation of Fe and Co in CuO host is not ordered. These results could be attributed to two main reasons. First, the ionic radii of  $\text{Cu}^{2+}$ ,  $\text{Fe}^{2+}$  and  $\text{Co}^{2+}$  are 0.072, 0.083, and 0.074 Å, respectively [37,57–59]. These values are close to each other and thereby Cu ions in the lattice structure can be well replaced by Fe and Co ions. The second reason is the complexity of the CuO monoclinic crystal structure and the anisotropic variation in the crystal lattice.

The random orientation of the atomic planes occurs in the growth of CuO thin films [7]. However, Fig. 1 clearly shows that the intensities of (002) and (200) peaks are much stronger than that of the other peaks. This may indicate some preferential orientations of the formed nanocrystals along these directions. The quantitative information concerning the preferential crystallite orientation is expressed by the well-known relation [51,60]:

$$\text{TC}_{(hkl)} = \frac{I}{I_0} \left[ \frac{1}{n} \sum \frac{I_{(hkl)}}{I_{0(hkl)}} \right]^{-1} \quad (3)$$

where TC is the texture coefficient,  $I_{(hkl)}$  is the measured intensity of a plane ( $hkl$ ),  $I_{0(hkl)}$  is the standard intensity of the plane ( $hkl$ ) taken from the JCPDS data, and  $n$  is the number of diffraction peaks. A sample with randomly oriented crystallites presents  $\text{TC}_{(hkl)} = 1$ , the larger this value, the larger abundance of crystallites oriented in the ( $hkl$ ) direction. The TCs values are calculated considering the first three peaks; (110), (002) and (200) and presented in Fig. 2. As seen,  $\text{TC}_{(002)}$  and  $\text{TC}_{(200)}$  are greater than unity and varied with the doping in a reverse behavior to each other.

#### Chemical composition and film morphology

Fig. 3 shows the energy dispersive X-ray spectroscopy (EDX/SEM) analyzes of pure CuO and 6% Fe-doped CuO thin film on the glass substrates. Qualitative and quantitative analyzes of the chemical composition of the fabricated CuO thin film is shown in Fig. 3(a). This EDX spectrum clearly confirms the presence of Cu and O peaks. There are two peaks relevant to Cu at around 1 keV and 8 keV. The quantitative analysis of the CuO is 79% Cu and 21% O, which indicates the high purity of the fabricated CuO thin film. However, the chart in Fig. 3(a) shows that the O signal not only comes from the CuO thin film but also from the glass substrate. In addition, Si, Ca, Mg and Na signals are detected from the glass substrate in the EDX pattern. The observed Cu and O ratios are affected by the preparation conditions. Alami et al. [61] prepared CuO films by submerging copper substrates in a

Table 1  
XRD data; full width at half maximum intensity (FWHM), crystallite size ( $C_s$ ),  $d$ -spacing, and the lattice parameters of the un-doped and Fe and Co doped CuO films.

Film	FWHM			$C_s$ (nm)	$d$ -Spacing			Lattice parameters			
	(110)	(002)	(200)		(110)	(002)	(200)	$a$ (Å)	$b$ (Å)	$c$ (Å)	$V$ (Å <sup>3</sup> )
CuO (pure)	0.945	0.472	0.236	20.44	2.758	2.528	2.334	4.734	3.418	5.127	81.82
CuO: 3% Fe	0.551	0.433	0.590	15.98	2.752	2.534	2.328	4.721	3.412	5.138	81.62
CuO: 6% Fe	0.551	0.315	0.551	18.72	2.766	2.530	2.327	4.718	3.441	5.131	82.17
6% Fe + 1.5% Co	0.6300	0.236	0.512	21.38	2.765	2.527	2.321	4.707	3.422	5.123	81.85
6% Fe + 3.0% Co	0.472	0.295	0.236	26.82	2.759	2.526	2.332	4.728	3.442	5.123	81.75

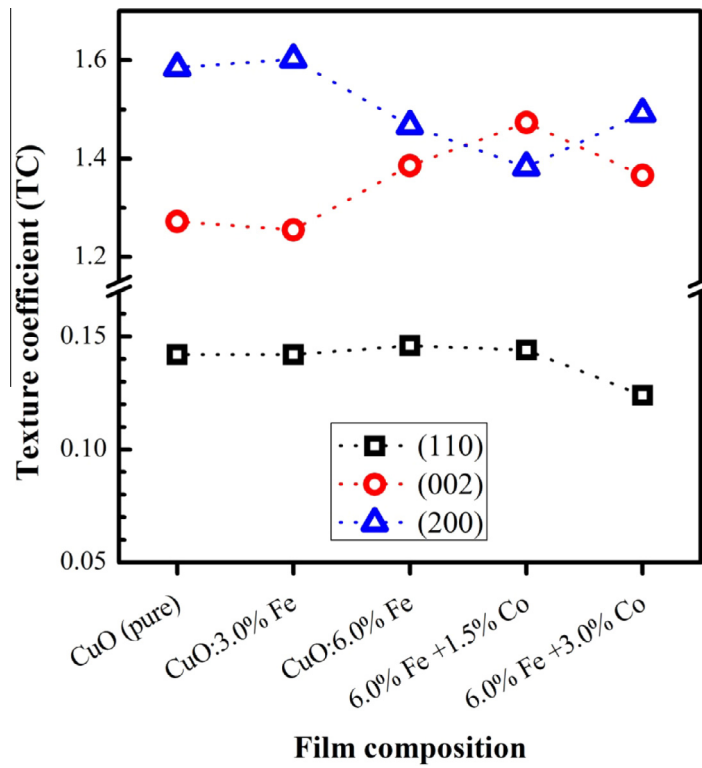


Fig. 2. The texture coefficients; TC(110), TC(002) and TC(200) according to the film composition.

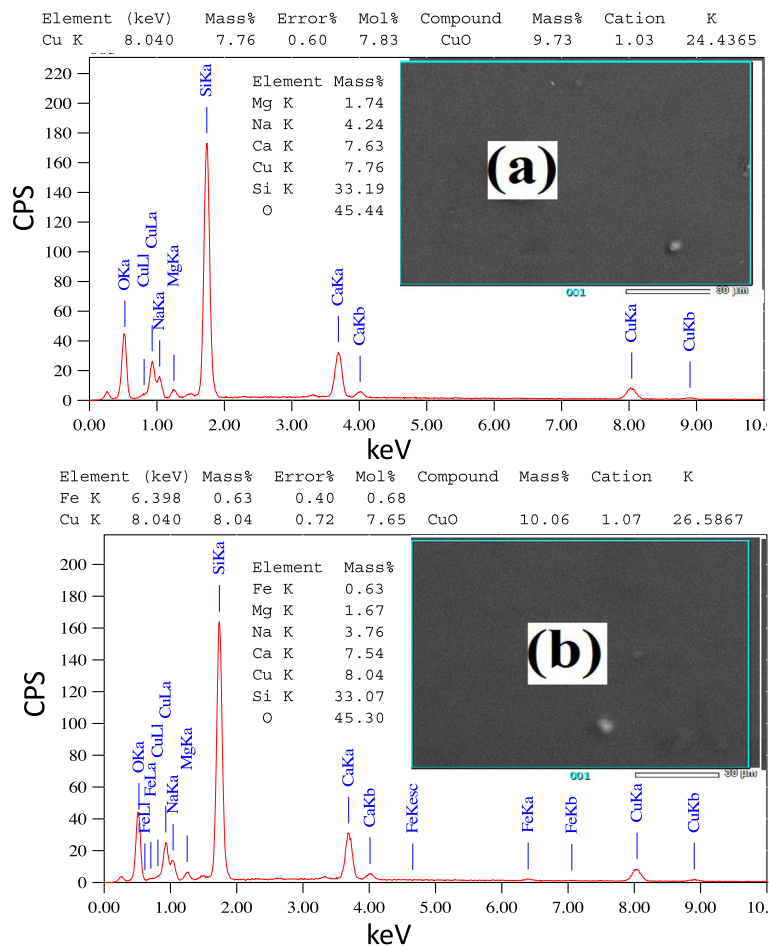


Fig. 3. EDX spectra of the (a) pure CuO and (b) 6% Fe-doped CuO film on glass substrate.

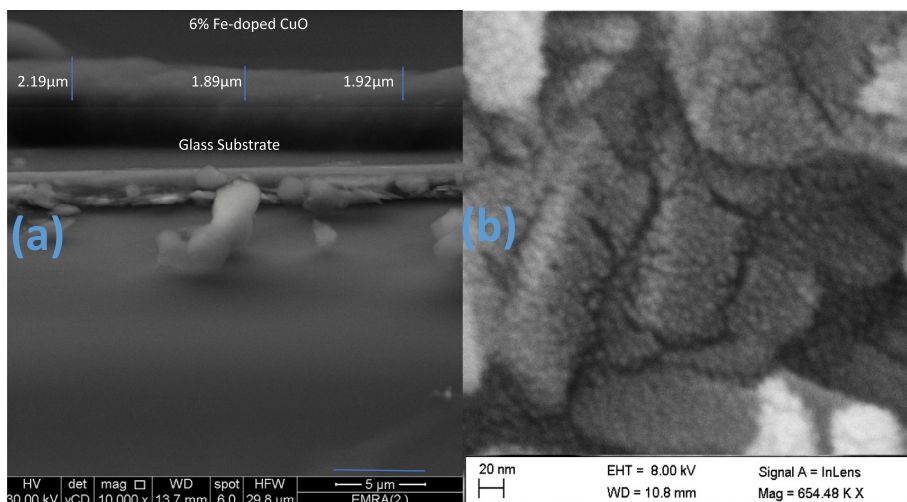


Fig. 4. SEM images of 6% Fe-doped CuO film on glass substrate (a) cross-sectional view and (b) top-view.

75 mmol/L ammonia solution at pH = 11 and at RT. The specimen that taken out after 36 h had showed 46.2% O versus 53.8% for Cu then became 49.3% O versus 50.7% Cu after 9 days.

The EDX spectrum of Fe-doped CuO film, Fig. 3(b), exhibited the same signals in Fig. 3(a) in addition to Fe signals. The quantitative analysis indicated that the ratio of Fe is 6%. For the co-doped film with Co, no signals are detected for Co and the observed signals are typical of EDX spectrum in Fig. 3(b). Fig. 4 illustrates SEM images of 6% Fe-doped CuO thin film on the glass substrate. From the cross-sectional SEM image in Fig. 4(a), the average thickness of the film is estimated to be  $\sim 2 \mu\text{m}$ . The surface morphology of the film is shown in the top-view field emission – SEM image in Fig. 4(b). This image demonstrates smooth film from agglomerated spherical NPs with tiny diameters ( $< 15 \text{ nm}$ ). These particles show a narrow size distribution and the number of particles per unit area is very high. So this film is suitable for nanotechnological applications such as sensors and photocatalysts.

#### Optical characterizations

The data of the normal transmittance  $T_t$  and reflectance  $R_t$  spectra taken from the equipment were corrected due to the substrate effects according to the formulas [62]

$$T_f = \frac{T_t T_s (1 - R_t R_s)}{T_s^2 - T_t^2 R_s^2} \quad (4)$$

$$R_f = \frac{R_t T_s^2 - T_t^2 R_s}{T_s^2 - T_t^2 R_s^2} \quad (5)$$

where  $T_f$  and  $R_f$  are the transmittance and reflectance of the film only, and  $T_s$  and  $R_s$  are the transmittance and reflectance of the used glass substrates. Fig. 5(a) shows the dependence of the corrected transmittance ( $T_f$ ) on the wavelength. As seen, the transmittance of the films increases almost linearly with the wavelength ( $\lambda$ ) of the incident radiation in the range 500–800 nm, then the spectra reach the maximum values around  $\lambda = 850 \text{ nm}$ . The values of  $T_f$  in the range  $\lambda = 600\text{--}800 \text{ nm}$  is between 21.5% and 70%. This is similar to the values obtained for CuO films deposited on glass substrates by thermal oxidation of metallic Cu films at 350–450 °C [13]. Also, it is observed that the film with the largest crystallite size, 6.0% Fe + 3.0% Co, showed the highest transparency. This result is similar to the results published by Oral et al. [24]. In a recent study, the CuO film fabricated by SILAR method exhibited transparency up to 80% at  $\lambda > 700 \text{ nm}$  only when doped with Mn [52]. Also, Joseph et al. [54] reported an enhancement in the transmittance for the spray deposited CuO films when doped with 10% Fe.

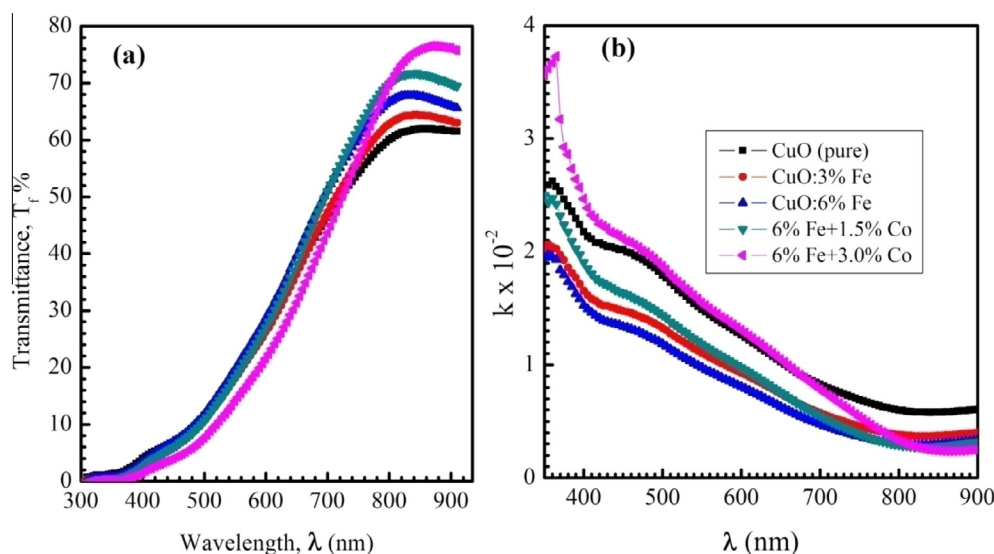


Fig. 5. (a) The transmittance spectra of the doped CuO films and (b) the dependence of the absorption index ( $k$ ) on the wavelength.

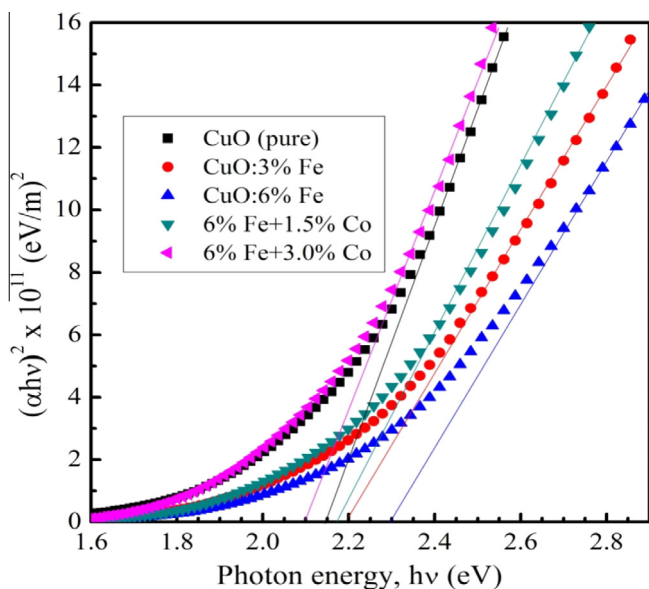


Fig. 6. The plots of  $(\alpha hv)^2$  vs. photon energy,  $h\nu$ , of the Fe- and Co co-doped CuO films.

Because of the crystallinity and relatively higher transparency, the copper oxide films are suitable for optical analysis from which the absorption coefficient and energy band gap can be determined. For the film of thickness  $t$ , both the absorption coefficient ( $\alpha$ ) and the absorption index ( $k$ ) were calculated using the relations [44]:

$$\alpha = \frac{1}{t} \ln \left( \frac{1}{T_f} \right) \quad \text{and} \quad k = \frac{\alpha \lambda}{4\pi} \quad (6)$$

The absorption index ( $k$ ) reflects the absorption of electromagnetic waves in the semiconductor due to inelastic scattering events [63]. Fig. 5(b) shows the dependence of  $k$  of the films on the wavelength. The  $k$  values are between 0.0024 and 0.037 and relatively constant in the long wavelength region, confirming the high transparency of the prepared films [64].

The theory of optical absorption gives the relationship between the absorption coefficient  $\alpha$  and the photon energy  $h\nu$  [7]:

$$\alpha = \frac{A(h\nu - E_g)^{n/2}}{h\nu} \quad (7)$$

where  $A$  is a constant,  $E_g$  is the optical band gap,  $h$  is the Planck's constant ( $6.625 \times 10^{-34}$  J/s), and  $n = 1$  for the direct allowed transition. The optical band gap,  $E_g$  values were obtained by extrapolating the linear part of the plots of  $(\alpha hv)^2$  vs.  $h\nu$  to  $\alpha = 0$ , as shown in Fig. 6. The linear portion that observed in this figure indicates that the transition is performed directly. The corresponding  $E_g$  values are given in Table 2. As seen from Fig. 6 and Table 2, the  $E_g$  values increased from 2.15 to 2.30 eV with the increasing of Fe doping ratio from 0% to 6.0%. Similar results were reported for CuO nanofibers [5] and also for the dip coated In-doped CuO films [9].

Table 2

The optical absorbance at 665 and 670 nm wavelength, the optical band gap ( $E_g$ ), the Urbach energy ( $E_U$ ), the minimum refractive index ( $n_{\min}$ ), the ratio of carrier concentration to the electron effective mass,  $(e^2/\pi c^2)(N/m^3)$ , the single oscillator energy ( $E_o$ ), and the energy parameter ( $E_d$ ) of the sol-gel spin coated CuO films.

Film	Abs. ( $\lambda = 665$ nm)	Abs. ( $\lambda = 670$ nm)	$E_g$ (eV)	$E_U$ (m eV)	$n_{\min}$	$(e^2/\pi c^2)(N/m^3)$ ( $\text{nm}^{-2}$ )	$E_o$ (eV)	$E_d$ (eV)
CuO (pure)	0.3616	0.3503	2.15	482	1.7658 (at 620 nm)	$5.91 \times 10^{-6}$	3.017	4.79
CuO: 3% Fe	0.3627	0.3502	2.20	407	1.8074 (at 670 nm)	$3.47 \times 10^{-6}$	3.145	4.56
CuO: 6% Fe	0.3264	0.3148	2.30	376	1.3702 (at 675 nm)	$3.14 \times 10^{-6}$	3.168	4.53
6% Fe + 1.5% Co	0.3381	0.3241	2.17	689	1.0129 (at 700 nm)	$9.81 \times 10^{-6}$	2.990	3.48
6% Fe + 3.0% Co	0.4197	0.4043	2.10	781	1.2821 (at 795 nm)	$1.35 \times 10^{-5}$	2.806	5.72

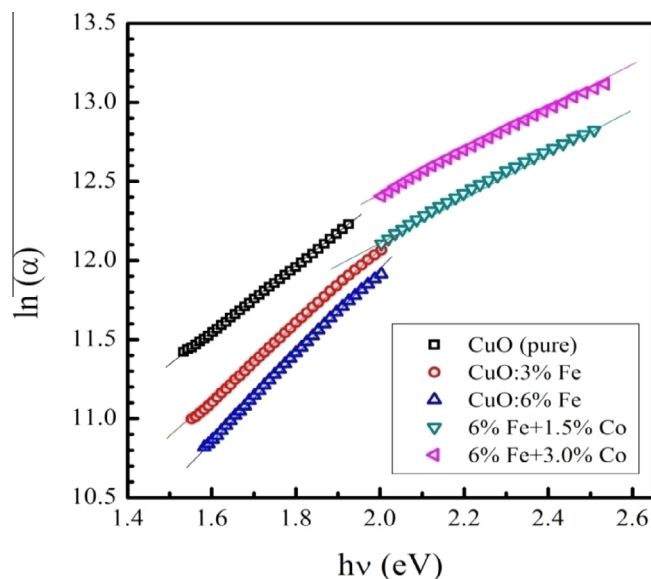


Fig. 7. The Urbach plot of the doped CuO films.

Sabbaghan et al. [12] prepared CuO NPs having  $E_g$  in the range 1.67–1.85 eV. Umadevi and Christy [29] reported  $E_g$  of about 3.0 eV for CuO nanoflowers. Basith et al. reported the increase of the  $E_g$  of CuO NPs from 2.8 eV to 3.4 eV with increasing Fe content from 0% to 2.0% wt. [10]. In addition,  $E_g$  of the doped CuO films prepared by SILAR method, continuously increased with increasing Mn content to 5% [52]. The observed blue shift may be originated from active transitions involving 3d levels in  $\text{Fe}^{2+}$  ions as well as the strong  $sp-d$  exchange interactions between the band electrons and the localized 'd' electrons of the Fe. On the other hand, the co-doping of CuO films with Co ions cause the decrease of  $E_g$  values. This shows an improvement of the quality of the films and supports the XRD results as the incorporation of Co ions enhances the grain growth process. This reverse relation between  $C_s$  and  $E_g$  was also reported for the In-doped CuO films that prepared by flame spray pyrolysis followed by spin coating [43] and for spray deposited CuO films [54]. In addition, Chaparro et al. and Hong et al., individually, illustrated that the red shift in the  $E_g$  of ZnSe [65] and ZnO [66] films was attributed to the increase in grain size of the prepared films.

The absorption coefficient,  $\alpha$  near the fundamental absorption edge (Urbach tail) usually shows simple exponential energy dependence according to the relation:

$$\alpha = \alpha_o \exp \left( \frac{h\nu}{E_U} \right) \quad (8)$$

where  $\alpha_o$  is a constant and  $E_U$  is the Urbach energy that determines the width of the tail.  $E_U$  is attributed to the disorder in the material that leads to the tail in the valence and conduction bands. Fig. 7 shows the plots of  $\ln(\alpha)$  vs. the photon energy ( $h\nu$ ) and the values

of  $E_U$  were obtained from the slopes of the linear fitting of this figure according to the relation:

$$E_U = \left[ \frac{d(\ln(\alpha))}{d(h\nu)} \right]^{-1} \quad (9)$$

The obtained  $E_U$  values are listed in Table 2. It is observed that, the  $E_U$  values are inversely changed with  $E_g$  of the films. Thus,  $E_U$  decreases with the increasing of Fe content and then increases with the co-doping with Co. Similar results were reported for Cu-doped ZnO thin films [57].

Evaluation of the refractive indices of the films is considerably important for the applications in integrated optics devices in which the refractive index is a key parameter for the device design. The complex refractive index is defined as  $\tilde{n} = n + ik$ , where the refractive index,  $n$ , given by [57,60]:

$$n = \frac{1 + R_f}{1 - R_f} + \sqrt{\frac{4R_f}{(1 - R_f)^2} - k^2} \quad (10)$$

Fig. 8 shows the dependence of  $n$  values on the wavelength  $\lambda$ , of the applied radiation. In the short wavelength region,  $n$  is constant and ranged from 1.5 to 2.2 depending on the doping ratio. With increasing  $\lambda$ , the  $n$  value decreases to a minimum value and then increases. It can be seen that at  $\lambda \geq 760$  nm, the value of  $n$  of the CuO films decreases with increasing the doping ratio (Fe and Co contents). Similar behaviors have been reported for CuO thin films prepared by the activated reactive evaporation method [67,68]. In addition, the wavelength corresponding to the minimum value of  $n$  shift to longer values with increasing the doping ratio, as given in Table 2.

From the normal dispersion behavior of  $n$  with  $\lambda$ , various dispersion parameters can be calculated. The ratio of carrier concentration to the electron effective mass ( $(e^2/\pi c^2)/(N/m^*)$ ) can be calculated by considering the dependence of  $n^2$  on  $\lambda^2$  (as shown in the inset of Fig. 8) according to the following dispersion relation [60]:

$$n^2 = \varepsilon_l - \left( \frac{e^2}{\pi c^2} \right) (N/m^*) \lambda^2 \quad (11)$$

where  $\varepsilon_l$  is the lattice dielectric constant. The obtained values of  $(e^2/\pi c^2)/(N/m^*)$  are given in Table 2. With the Fe incorporation

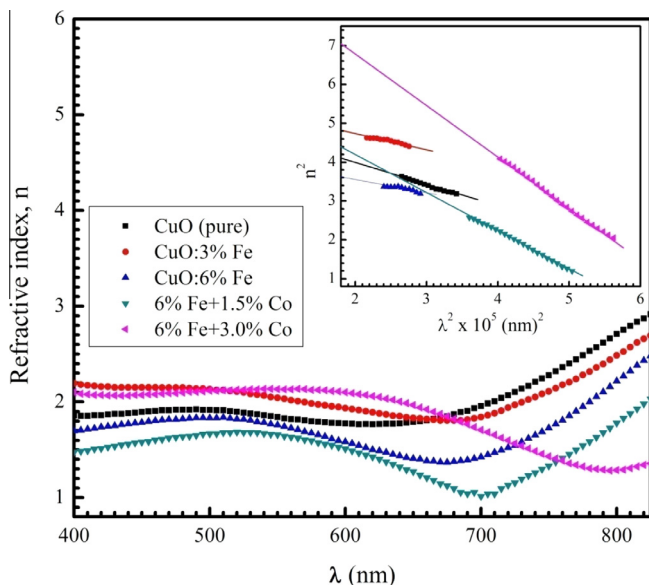


Fig. 8. The dependence of the refractive index  $n$  on  $\lambda$ . The inset shows the dependence on  $n^2$  on  $\lambda^2$  according to Eq. (11).

within CuO films, the ratio of carrier concentration to the electron effective mass is decreased and then increased with the co-doping with Co. This is consistent with the variation in the  $E_g$  values by increasing Fe and Co content, where,  $E_g$  values increase (decrease) with decreasing (increasing) the carrier concentrations [69].

In the low absorption region, the relation between the refractive index and the oscillator strength below the band gap is given by:

$$n^2 = 1 + \frac{E_d E_o}{E_o^2 - (h\nu)^2} \quad (12)$$

where  $E_o$  is the oscillator energy and  $E_d$  is the dispersion energy which is a measure of the strength of interband optical transitions. The values of  $E_d$  and  $E_o$  can be obtained from the intercept and slope of the linear fitted lines by plotting  $(n^2 - 1)^{-1}$  vs.  $(h\nu)^2$ , as depicted in Fig. 9. The obtained values of  $E_d$  and  $E_o$  are listed in Table 2. The oscillation energy can be correlated with the optical gap by the empirical formula  $E_o = 1.38 E_g$ . Based on these results, it can suggest that the optical constants of the CuO films could be controlled by Fe and co-doping with Co. The quantitative measurements of these parameters may help in tailoring and modeling the properties of such films for their use in optoelectronic components and devices.

#### Photocatalytic properties

The photodegradation efficiency ( $\eta$ ) was calculated from the decrease of the absorbance of the MB dye solution at its maximum absorption wavelength (668 nm) as follows:

$$\eta = \frac{C_o - C_t}{C_o} \times 100 \quad (13)$$

where  $C_o$  represents the initial concentration of the dye solution and  $C_t$  represents the concentration of the dye at solar light irradiation time ( $t$ ). Fig. 10 shows the degradation efficiency (% removal) as a function of the light exposure time for the films: CuO (pure), CuO: 6% Fe, and 6.0% Fe + 3.0% Co. As seen, the co-doping with Co cause 100% removal compared to 95.6% removal for CuO (pure) and 94.9% removal for CuO: 6% Fe after 12 h exposure to the

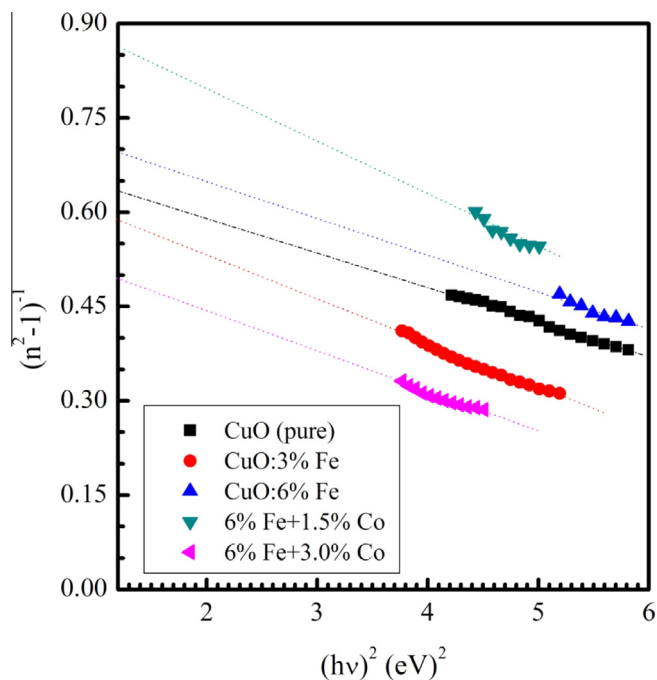
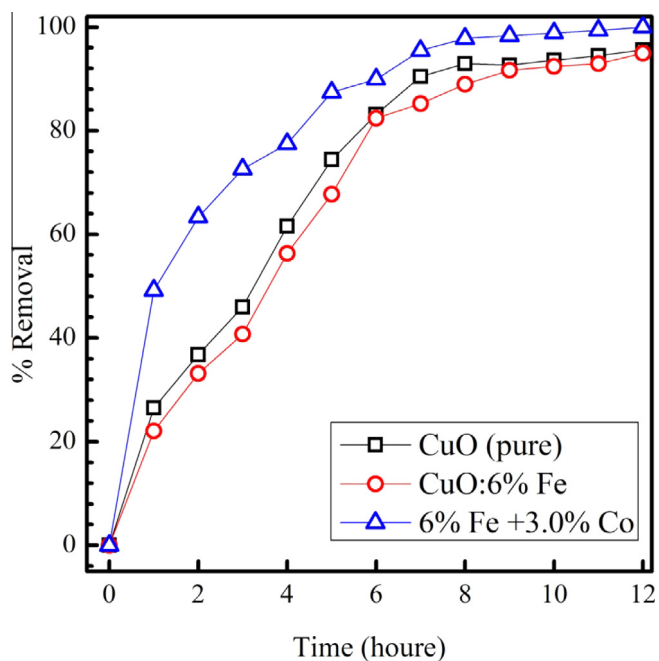
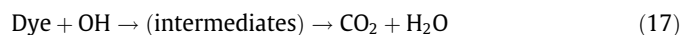


Fig. 9. The variation of  $(n^2 - 1)^{-1}$  w.r.t.  $(h\nu)^2$  for pure CuO, Fe-doped and Fe-and Co co-doped CuO films.



**Fig. 10.** The degradation efficiency (% removal) for CuO, CuO: 6% Fe, and 6.0% Fe + 3.0% Co films.

sunlight. The proposed reaction mechanism can be illustrated as follows:



The absorbance values of the CuO films at  $\lambda = 665$  and  $670$  nm are given in Table 2 in the previous section. It can be seen that 6% Fe + 3.0% Co film have an absorbance value higher than that of CuO: 6% Fe. As the Fe concentration increases,  $E_g$  of CuO increases and therefore not more photons can penetrate  $E_g$  to create the  $(e^-, h^+)$  pairs. Hence, fewer amounts of the hydroxyl radicals (OH) are generated and the photodegradation efficiency is reduced [45]. However, co-doping of CuO films with Co leads to the reduction of  $E_g$ . This enables more photons to penetrate the  $E_g$  resulting in the increase in  $(e^-, h^+)$  pairs creation and the production of  $\text{OH}$ . This leads to the increase of MB degradation [70]. Similar results were reported; Sohrabnezhad et al. [15] demonstrated that CuO-montmorillonite (MMT) nanocomposite has a higher bactericidal effect than that of MMT alone. The electrochemically synthesized CuO thin films of nanowhiskers-like structure showed good efficiency in removal of Rose Bengal (RB) dye from the waste water [27]. Also, the rod-like CuO effectively degraded the Coomassie brilliant blue R-250 dye beneath the sunlight [28]. Umadevi and Christy reported the good photocatalytic activity of CuO nanoflowers for the removal of methyl orange (MO) under UV irradiation [29]. Also, CuO–ZnO mixed oxide showed a good efficiency in degrading C.I. Reactive Orange 16 (V3R) in water due to increasing the number of surface active sites for the interaction [71]. All of these results confirm the effective use of CuO nanocomposite materials in the photocatalytic degradation of various dyes.

## Conclusions

High purity and nanostructured CuO films doped with Fe and co-doped with Co have been synthesized successfully by applying the sol–gel spin coating technique. XRD results revealed that the prepared films were of polycrystalline nature with  $C2/c$  space group. The incorporation of Fe and Co did not change the monoclinic structure of CuO. The films showed transparency between 21.5 and 70% in the most of the visible region of the spectra. The band gap of CuO films can be tuned between 2.1 and 2.3 eV by doping with Fe and Co. The optical constant such as the absorption index, refractive index, the ratio of carrier concentration to the electron effective mass, single oscillator energy could be controlled by the Fe doping and co-doping with Co. The photocatalytic degradation of methylene blue (MB) by CuO films showed lower enhancement than when Co was incorporated into CuO: 6% Fe. In conclusion, the proposed method has some merits like the low cost of processing, facile technology, high controllability, and relatively simple equipment. All of these factors facilitate the use of the prepared films in optoelectronic components and devices.

## References

- [1] F.K. Mugwang'a, P.K. Karimi, W.K. Njoroge, O. Omayio, S.M. Waita, Optical characterization of Copper Oxide thin films prepared by reactive dc magnetron sputtering for solar cell applications, *Int. J. Thin Film Sci. Tec.* 2 (2013) 15–24.
- [2] A. Subramaniyan, J.D. Perkins, R.P. O'Hayre, S. Lany, V. Stevanovic, D.S. Ginley, A. Zakutayev, Non-equilibrium deposition of phase pure  $\text{Cu}_2\text{O}$  thin films at reduced growth temperature, *APL Mater.* 2 (2014) 022105.
- [3] S.Y. Kim, C.H. Ahn, J.H. Lee, Y.H. Kwon, S. Hwang, J.Y. Lee, H.K. Cho, P-channel oxide thin film transistors using solution-processed copper oxide, *ACS Appl. Mater. Interfaces* 5 (2013) 2417–2421.
- [4] M.R. Johan, M.S.M. Suan, N.L. Hawari, H.A. Ching, Annealing effects on the properties of copper oxide thin films prepared by chemical deposition, *Int. J. Electrochem. Sci.* 6 (2011) 6094–6104.
- [5] R. Sahay, J. Sundaramurthy, P. Suresh Kumar, V. Thavasi, S.G. Mhaisalkar, S. Ramakrishna, Synthesis and characterization of CuO nanofibers, and investigation for its suitability as blocking layer in ZnO NPs based dye sensitized solar cell and as photocatalyst in organic dye degradation, *J. Solid State Chem.* 186 (2012) 261–267.
- [6] Y. Caglar, D.D. Oral, M. Caglar, S. Ilican, M.A. Thomas, K. Wu, Z. Sun, J. Cui, Synthesis and characterization of  $(\text{CuO})_x(\text{ZnO})_{1-x}$  composite thin films with tunable optical and electrical properties, *Thin Solid Films* 520 (2012) 6642–6647.
- [7] D.M. Jundale, P.B. Joshi, S. Sen, V.B. Patil, Nanocrystalline CuO thin films: synthesis, microstructural and optoelectronic properties, *J. Mater. Sci.: Mater. Electron.* 23 (2012) 1492–1499.
- [8] N.M. Basith, J.J. Vijaya, L.J. Kennedy, M. Bououdina, Structural, morphological, optical, and magnetic properties of Ni-doped CuO nanostructures prepared by a rapid microwave combustion method, *Mater. Sci. Semicond. Process.* 17 (2014) 110–118.
- [9] A. Yildiz, S. Horzum, N. Serin, T. Serin, Hopping conduction in In-doped CuO thin films, *Appl. Surf. Sci.* 318 (2014) 105–107.
- [10] N.M. Basith, J.J. Vijaya, L.J. Kennedy, M. Bououdina, Structural, optical and room-temperature ferromagnetic properties of Fe-doped CuO nanostructures, *Phys. E* 53 (2013) 193–199.
- [11] S. Horzum, A. Yildiz, N. Serin, T. Serin, Carrier transport in In-doped CuO thin films, *Philos. Mag.* 93 (2013) 3110–3117.
- [12] M. Sabbaghan, A.S. Shahvelayati, K. Madankar, CuO nanostructures: Optical properties and morphology control by pyridinium-based ionic liquids, *Spectrochim. Acta A* 135 (2015) 662–668.
- [13] V. Figueiredo, E. Elangovan, G. Goncalves, P. Barquinha, L. Pereira, N. Franco, E. Alves, R. Martins, E. Fortunato, Effect of post-annealing on the properties of copper oxide thin films obtained from the oxidation of evaporated metallic copper, *Appl. Surf. Sci.* 254 (2008) 3949–3954.
- [14] Y.S. Chaudhary, A. Agrawal, R. Shrivastav, V.R. Satsangi, S. Dass, A study on the photoelectrochemical properties of copper oxide thin films, *Int. J. Hydrogen Energy* 29 (2004) 131–134.
- [15] Sh. Sohrabnezhad, M.J.M. Moghaddam, T. Salavatiyan, Synthesis and characterization of CuO–montmorillonite nanocomposite by thermal decomposition method and antibacterial activity of nanocomposite, *Spectrochim. Acta A* 125 (2014) 73–78.
- [16] P. Samarasekara, N.T.R.N. Kumara, N.U.S. Yapa, Sputtered copper oxide (CuO) thin films for gas sensor devices, *J. Phys-Condens. Mater.* 18 (2006) 2417–2420.
- [17] D. Jundale, S. Pawar, M. Chougule, P. Godse, S. Patil, B. Raut, S. Sen, V. Patil, Nanocrystalline CuO thin films for H<sub>2</sub>S monitoring: microstructural and optoelectronic characterization, *J. Sensor Technol.* 1 (2011) 36–46.

- [18] H.T. Hsueh, T.J. Hsueh, S.J. Chang, F.Y. Hung, T.Y. Tsai, W.Y. Weng, C.L. Hsu, B.T. Dai, CuO nanowire-based humidity sensors prepared on glass substrate, *Sensor Actuators B – Chem.* 156 (2011) 906–911.
- [19] G. Zhu, H. Xu, Y. Xiao, Y. Liu, A. Yuan, X. Shen, Facile fabrication and enhanced sensing properties of hierarchically porous CuO architectures, *ACS Appl. Mater. Interfaces* 4 (2012) 744–751.
- [20] K. Jindal, M. Tomar, V. Gupta, CuO thin film based uric acid biosensor with enhanced response characteristics, *Biosens. Bioelectron.* 38 (2012) 11–18.
- [21] L. Zhang, F. Yuan, X. Zhang, L. Yang, Facile synthesis of flower like copper oxide and their application to hydrogen peroxide and nitrite sensing, *Chem. Cent. J.* 5 (2011) 75, <http://dx.doi.org/10.1186/1752-153X-5-75>.
- [22] A. Taubert, F. Stange, Z. Li, M. Junginger, C. Gunter, M. Neumann, A. Friedrich, CuO nanoparticles from the strongly hydrated ionic liquid precursor (ILP) tetrabutylammonium hydroxide: evaluation of the ethanol sensing activity, *ACS Appl. Mater. Interfaces* 4 (2012) 791–795.
- [23] J.S. Shaikh, R.C. Pawar, R.S. Devan, Y.R. Ma, P.P. Salvi, S.S. Kolekar, P.S. Patil, Synthesis and characterization of Ru doped CuO thin films for supercapacitor based on Bronsted acidic ionic liquid, *Electrochim. Acta* 56 (2011) 2127–2134.
- [24] A.Y. Oral, E. Mensur, M.H. Aslan, E. Basaran, The preparation of copper(II) oxide thin films and the study of their microstructures and optical properties, *Mater. Chem. Phys.* 83 (2004) 140–144.
- [25] Y. Liu, L. Liao, J. Li, C. Pan, From copper nanocrystalline to CuO nanoneedle array: synthesis, growth mechanism, and properties, *J. Phys. Chem. C* 111 (2007) 5050–5056.
- [26] M.H. Habibi, B. Karimi, M. Zendehtdel, M. Habibi, Fabrication, characterization of two nano-composite CuO–ZnO working electrodes for dye-sensitized solar cell, *Spectrochim. Acta A* 116 (2013) 374–380.
- [27] N. Mukherjee, B. Show, S.K. Maji, U. Madhu, S.K. Bhar, B.C. Mitra, G.G. Khan, A. Mondal, CuO nano-whiskers: electrodeposition, Raman analysis, photoluminescence study and photocatalytic activity, *Mater. Lett.* 65 (2011) 3248–3250.
- [28] R. Sankar, P. Manikandan, V. Malarvizhi, T. Fathima, K.S. Shivashangari, V. Ravikumar, Green synthesis of colloidal copper oxide nanoparticles using Carica papaya and its application in photocatalytic dye degradation, *Spectrochim. Acta A* 121 (2014) 746–750.
- [29] M. Umadevi, A.J. Christy, Synthesis, characterization and photocatalytic activity of CuO nanoflowers, *Spectrochim. Acta A* 109 (2013) 133–137.
- [30] R. Sivaraj, P.K.S.M. Rahman, P. Rajiv, S. Narendhran, R. Venkatesh, Biosynthesis and characterization of *Acalypha indica* mediated copper oxide nanoparticles and evaluation of its antimicrobial and anticancer activity, *Spectrochim. Acta A* 129 (2014) 255–258.
- [31] R. Sivaraj, P.K.S.M. Rahman, P. Rajiv, H. Abdul Salam, R. Venkatesh, Biogenic copper oxide nanoparticles synthesis using *Tabernaemontana divaricate* leaf extract and its antibacterial activity against urinary tract pathogen, *Spectrochim. Acta A* 133 (2014) 178–181.
- [32] A.P. Moura, L.S. Cavalcante, J.C. Sczancoski, D.G. Stroppa, E.C. Paris, A.J. Ramirez, J.A. Varela, E. Longo, Structure and growth mechanism of CuO plates obtained by microwave-hydrothermal without surfactants, *Adv. Powder Technol.* 21 (2010) 197–202.
- [33] F. Zhao, H.M. Qiu, L.Q. Pan, H. Zhu, Y.P. Zhang, Z.G. Guo, J.H. Yin, X.D. Zhao, J.Q. Xiao, Ferromagnetism analysis of Mn-doped CuO thin films, *J. Phys.-Condens. Mat.* 20 (2008) 425208.
- [34] Y. Zhang, L. Pan, Y. Gu, F. Zhao, H. Qiu, J. Yin, H. Zhu, J.Q. Xiao, Metal-insulator transition in ferromagnetic Mn-doped CuO thin films, *J. Appl. Phys.* 105 (2009) 086103.
- [35] H. Zhu, F. Zhao, L. Pan, Y. Zhang, C. Fan, Y. Zhang, J.Q. Xiao, Structural and magnetic properties of Mn-doped CuO thin films, *J. Appl. Phys.* 101 (2007) 09H111.
- [36] K.L. Liu, S.L. Yuan, H.N. Duan, X.F. Zheng, S.Y. Yin, Z.M. Tian, C.H. Wang, S.X. Huo, Exchange bias in Fe and Ni co doped CuO nanocomposites, *J. Appl. Phys.* 107 (2010) 023911.
- [37] S. Manna, S.K. De, Room temperature ferromagnetism in Fe doped CuO nanorods, *J. Magnet. Magnet. Mater.* 322 (2010) 2749–2753.
- [38] R.N. Mariammal, K. Ramachandran, G. Kalaiselvan, S. Arumugam, B. Renganathan, D. Sastikumar, Effect of magnetism on the ethanol sensitivity of undoped and Mn-doped CuO nanoflakes, *Appl. Surf. Sci.* 270 (2013) 545–552.
- [39] S. Lee, S.U.-S. Choi, S. Li, J.A. Eastman, Measuring thermal conductivity of fluids containing oxide nanoparticles, *J. Heat Transfer* 121 (1999) 280–289.
- [40] Q. Zhang, K. Zhang, D. Xu, G. Yang, H. Huang, F. Nie, C. Liu, S. Yang, CuO nanostructures: synthesis, characterization, growth mechanisms, fundamental properties and applications, *Progr. Mater. Sci.* 60 (2014) 208–337.
- [41] M.-Hui Chang, H.-Shen Liu, C.Y. Tai, Preparation of copper oxide nanoparticles and its application in nanofluid, *Powder Technol.* 207 (2011) 378–386.
- [42] C.C. Vidyasagar, Y.A. Naik, T.G. Venkatesh, R. Viswanatha, Solid-state synthesis and effect of temperature on optical properties of Cu–ZnO, Cu–CdO and CuO nanoparticles, *Powder Technol.* 214 (2011) 337–343.
- [43] P. Mallick, S. Sahu, Structure, microstructure and optical absorption analysis of CuO nanoparticles synthesized by sol–gel route, *Nanosci. Nanotechnol.* 2 (2012) 71–74.
- [44] C.-Ying Chiang, Y. Shin, S. Ehrman, Li doped CuO film electrodes for photoelectrochemical cells, *J. Electrochem. Soc.* 159 (2012) B227–B231.
- [45] R. Sathyamoorthy, K. Mageshwari, Synthesis of hierarchical CuO microspheres: photocatalytic and antibacterial activities, *Phys. E* 47 (2013) 157–161.
- [46] J. Jayaprakash, N. Srinivasan, P. Chandrasekaran, E.K. Giriya, Synthesis and characterization of cluster of grapes like pure and Zinc-doped CuO nanoparticles by sol–gel method, *Spectrochim. Acta A* 136 (2015) 1803–1806.
- [47] F. Bayansal, H.A. Cetinkara, S. Kahraman, H.M. Cakmak, H.S. Guder, Nanostructured CuO films prepared by simple solution methods: plate-like, needle-like and network-like architectures, *Ceram. Int.* 38 (2012) 1859–1866.
- [48] D. Gao, G. Yang, J. Li, J. Zhang, J. Zhang, D. Xue, Room-temperature ferromagnetism of flowerlike CuO nanostructures, *J. Phys. Chem. C* 114 (2010) 18347–18351.
- [49] P. Chand, A. Gaur, A. Kumar, Structural, optical and ferroelectric behavior of CuO nanostructures synthesized at different pH values, *Superlatt. Microstruct.* 60 (2013) 129–138.
- [50] T. Serin, A. Yildiz, S.H. Sahin, N. Serin, Multiphonon hopping of carriers in CuO thin films, *Physica B* 406 (2011) 3551–3555.
- [51] I. Singh, R.K. Bedi, Studies and correlation among the structural, electrical and gas response properties of aerosol spray deposited self assembled nanocrystalline CuO, *Appl. Surf. Sci.* 257 (2011) 7592–7599.
- [52] Y. Gulen, F. Bayansal, B. Sahin, H.A. Cetinkara, H.S. Guder, Fabrication and characterization of Mn-doped CuO thin films by the SILAR method, *Ceram. Int.* 39 (2013) 6475–6480.
- [53] A. Nalbant, O. Ertek, I. Okur, Producing CuO and ZnO composite thin films using the spin coating method on microscope glasses, *Mater. Sci. Eng., B* 178 (2013) 368–374.
- [54] D.P. Joseph, C. Venkateswaran, Effect of Fe alloying on the structural, optical, electrical and magnetic properties of spray-deposited CuO thin films, *J. Korean Phys. Soc.* 61 (2012) 449–454.
- [55] A. Arunachalam, S. Dhanapandian, C. Manoharan, G. Sivakumar, Physical properties of Zn doped TiO<sub>2</sub> thin films with spray pyrolysis technique and its effects in antibacterial activity, *Spectrochim. Acta A* 138 (2015) 105–112.
- [56] B. Rajamannan, S. Mugundan, G. Viruthagiri, P. Praveen, N. Shanmugam, Linear and nonlinear optical studies of bare and copper doped TiO<sub>2</sub> nanoparticles via sol gel technique, *Spectrochim. Acta A* 118 (2014) 651–656.
- [57] A.M. El Sayed, G. Said, S. Taha, A. Ibrahim, F. Yakuphanoglu, Influence of copper incorporation on the structural and optical properties of ZnO nanostructured thin films, *Superlatt. Microstruct.* 62 (2013) 47–58.
- [58] C. Russel, A. Wiedenroth, The effect of glass composition on the thermodynamics of the Fe<sup>2+</sup>/Fe<sup>3+</sup> equilibrium and the iron diffusivity in Na<sub>2</sub>O/MgO/CaO/Al<sub>2</sub>O<sub>3</sub>/SiO<sub>2</sub> melts, *Chem. Geology* 213 (2004) 125–135.
- [59] A.A. Ati, Z. Othaman, A. Samavati, Influence of cobalt on structural and magnetic properties of nickel ferrite nanoparticles, *J. Mol. Struct.* 1052 (2013) 177–182.
- [60] A.H. Alami, A. Allagui, H. Alawadhi, Microstructural and optical studies of CuO thin films prepared by chemical ageing of copper substrate in alkaline ammonia solution, *J. Alloys Compd.* 617 (2014) 542–546.
- [61] A.M. El Sayed, A. Ibrahim, Structural and optical characterizations of spin coated cobalt-doped cadmium oxide nanostructured thin films, *Mater. Sci. Semicond. Process.* 26 (2014) 320–328.
- [62] A.A. Akl, Influence of preparation conditions on the dispersion parameters of sprayed iron oxide thin films, *Appl. Surf. Sci.* 256 (2010) 7496–7503.
- [63] A.A. Ziabari, F.E. Ghodsi, Growth, characterization and studying of sol–gel derived CdS nanocrystalline thin films incorporated in polyethyleneglycol: effects of post-heat treatment, *Solar Energ. Mat. Sol. C.* 105 (2012) 249–262.
- [64] A.A.M. Farag, I.S. Yahia, F. Yakuphanoglu, M. Kandaz, W.A. Ferooq, Optical properties and the dispersion parameters of new zinc Phthalocyanine benzofuran derivative prepared by non-vacuum spin coating technique, *Opt. Commun.* 285 (2012) 3122–3127.
- [65] A.M. Chaparro, M.A. Martinez, C. Guillen, R. Bayon, M.T. Gutierrez, J. Herrero, SnO<sub>2</sub> substrate effects on the morphology and composition of chemical bath deposited ZnSe thin films, *Thin Solid Films* 361–362 (2000) 177–182.
- [66] R. Hong, J. Huang, H. He, Z. Fan, J. Shao, Influence of different post-treatments on the structure and optical properties of zinc oxide thin films, *Appl. Surf. Sci.* 242 (2005) 346–352.
- [67] B. Balamurugan, B.R. Mehta, Optical and structural properties of nanocrystalline copper oxide thin films prepared by activated reactive evaporation, *Thin Solid Films* 396 (2001) 90–96.
- [68] G. Papadimitropoulos, N. Vourdas, V.E. Vamvakas, D. Davazoglou, Deposition and characterization of copper oxide thin films, *J. Phys. Conference Series* 10 (2005) 182–185.
- [69] H.M. Ali, H.A. Mohamed, M.M. Wakkad, M.F. Hasaneen, Properties of transparent conducting oxides formed from CdO alloyed with In<sub>2</sub>O<sub>3</sub>, *Thin Solid Films* 515 (2007) 3024–3029.
- [70] Y.A. Shaban, Enhanced Photocatalytic Removal of Methylene Blue From Seawater Under Natural Sunlight Using Carbon-Modified n-TiO<sub>2</sub> Nanoparticles, *Environ. Poll.* 3 (2014) 41–50.
- [71] M.H. Habibi, B. Karimi, Nanostructure Cu–Zn mixed-oxide supported photocatalyst fabricated by impregnation method for the photocatalytic degradation of C.I. Reactive Orange 16 (V3R) in water, *Spectrochim. Acta A* 124 (2014) 629–631.